Chapter 6

Spectral synthesis

Contents

6.1 Effect of atmospheric inhomogeneities

Fig. 6.1 shows the predicted variations of the FeI artificial line ($\lambda = 5000.0$ Å, $\log(gf)$=-6.5 and χ=2.0 eV, see Tab. 3.3) across the granulation pattern of a RSG simulation (st35gm03n07 in Tab. 4.1). For the sake of simplicity, only the FeI line is computed to avoid the molecular blends in the spectra.

The different line contribution from different positions on the disk appear asymmetric and sometimes even doubled peaked (Fig. 6.1, top left panel) The line centers span values between -10 km/s and +7 km/s with respect to the hydrostatic model (black dashed line). Redshifted FeI lines correspond to regions where the gas is receding and blueshifted lines to regions where the gas is approaching the observer (see bottom right panel of the Figure: the velocity field averaged with the contribution function to the spectral line depression - Sect. 4.1). The resulting average (black solid line) has a quite complicated profile. The strength of lines computed from RHD models may differ from their one-dimensional counterparts (black dashed line in Fig. 6.1) for three reasons: (i) a different mean atmospheric structure, (ii) the existence of atmospheric inhomogeneities, and (iii) the velocity field in the atmosphere. In order to test if the velocity fields are the dominant explanation to the difference, I have calculated the same spectral line describe above setting all the velocities to 0 in the RHD model (bottom left panel). Line doubling and broadening have disappeared but still, the line strength of the one-dimensional model

spectrum and the three-dimensional one are different. Atmospheric inhomogeneities and mean structure contribute also to the difference.
The temperature profiles in top right panel show the sampling in optical depth for each calculated rays.

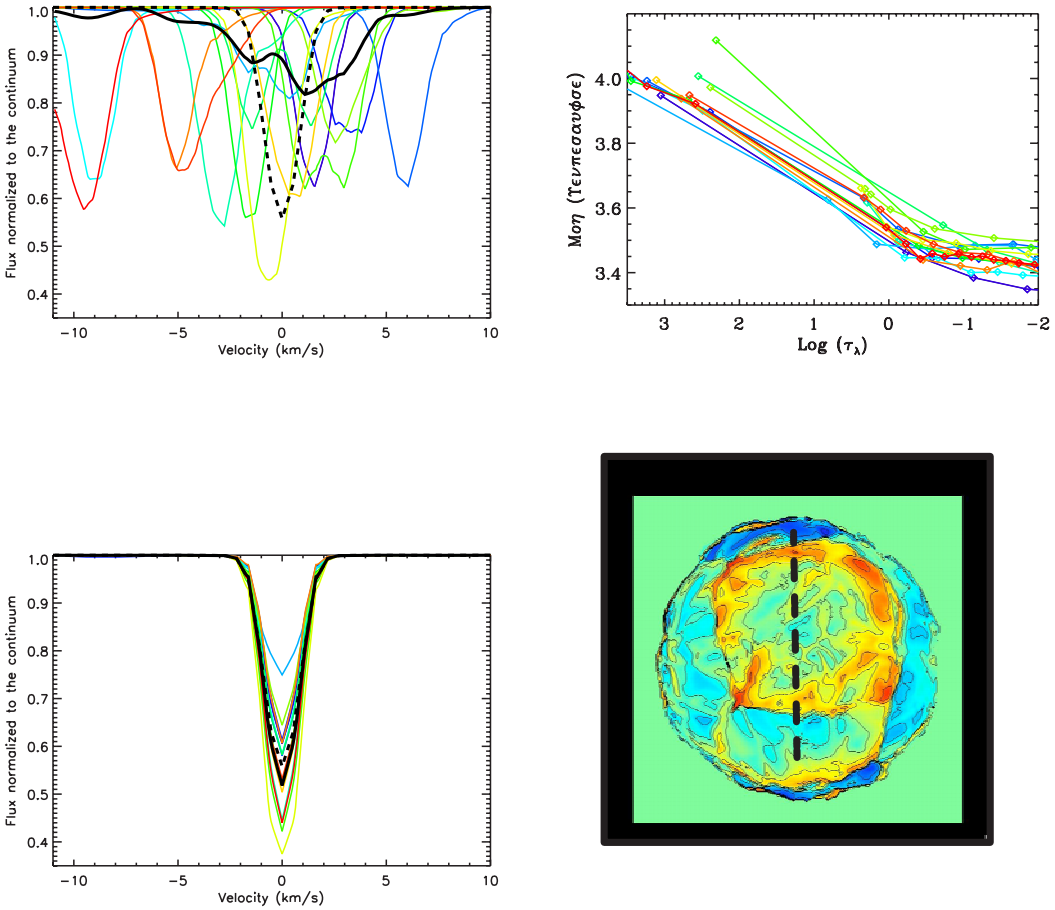

Figure 6.1: *Top left panel:* predicted variations of the FeI artificial line (λ = 5500.0 Å, log(gf)=-6.5 and χ=2.0 eV, see Tab. 3.3) across the granulation pattern of a RSG simulation (st35gm03n07 in Tab. 4.1). The resolution for the calculation is 0.05 km/s. The black solid curve is the averaged line profile and the black dashed curve is the synthetic spectrum obtained from a one-dimensional MARCS model with T_{eff}=3500K, surface gravity equal to -0.5 and solar metallicity. *Top right panel:* temperature profile as a function of the logarithmic optical depth computed for the corresponding ray in the cube. Colors have the same meaning as in top left panel. *Bottom left panel:* predicted variations of the FeI artificial line as in top left panel but with all the velocities set to 0 in the RHD simulation. *Bottom right panel:* Velocity field averaged with the contribution function to the spectral line flux depression (Sect. 4.1) at 5500 Å. Red corresponds to receding gas, blue to approaching gas and green is velocity=0. The velocity scale is (-20,+20) km/s. The black contour plot is the velocity contour plot. The vertical dashed line shows where the synthetic spectra have been calculated.

6.2 Comparison with observations

6.2.1 CO lines at 2.3 μm

Due to the large veiling by the molecules in the optical, the isolation of one line is easier in the IR region of the spectrum. The vibration-rotation bands of CO molecule (first overtone $\Delta v = 2$) offer a sequences of well separated spectral lines of different strengths. These line can be used to explore the dynamics at different depths in the atmosphere.
A detailed comparison in the K band has been done with the α Ori observation by Wallace & Hinkle (1996). Fig. 6.2 () shows two CO lines with different excitation potential. The strong line has $\lambda = 23094.369$ Å, $\log(gf)$=-5.262 and χ=0.120 eV, while the weaker line has $\lambda = 23097.094$ Å, $\log(gf)$=-4.195 and χ=1.476 eV.
In the Figure (top left panel), the RHD simulation (colored lines, st35gm03n07 in Tab. 4.1) approximately reproduces the width (but not fully) and depth of the weak line without invoking any free parameters such as micro-or macroturbulence that is always necessary in 1D modeling. The physical explanation for these parameters is in the Doppler shifts due to the convective motions. It is not possible to reproduce the strong and the weak line with the same model.
Three reasons may explain this difference: (i) the strong line could be partially formed above the photosphere and Non-LTE effect should be considered; (ii) the simulation used is the closest available to the α Ori effective temperature, but is, indeed, too cool ($T_{\rm eff} \sim 3495$K) with respect to the expected value (3650K, Levesque et al. 2005); (iii) a stratification dependance of the micro-turbulence.
In all my calculations presented in this work, I have used a micro-turbulence of 0 km/s and I did not find any evidence of need of a micro-turbulence. In this case, I have carried out some tests in order to reproduce the observed CO lines. Thus, I have generated some opacity tables that include (gaussian) microturbulence $\xi_t = 1.5, 2.5, 5$ km/s and I have computed synthetic spectra from model st35gm03n07. In Figure 6.2 (top right and bottom panels), it is evident that increasing the microturbulent parameter up to 5 km/s the strong line width is reproduced but the depth is still not fully fitted. The synthetic line profile appear asymmetric. However, the calculated weaker line becomes too strong with respect to the photospheric observed line. Passing from 0 to 5 km/s the line depths increase by $\sim 70\%$ both for the strong and weak line. The line depth and broadening are strongly dependent on the micro-turbulence velocity introduced.
In the literature, there are some observational evidence for a depth dependance of the turbulent parameter (e.g., Gray 1977, Gray 1982 and Gray 1988). In this case, the two CO lines form at different depths in the atmosphere and I have shown that a spectrum calculated using opacity tables with $\xi_t = 5$ km/s can approximately explain the strong line while there is no need of ξ_t for the weak line. However, this is not enough to firmly establish the existence of a depth dependance of the micro-turbulence and, furthermore, the strong line may experience Non-LTE effects. Different CO lines (and/or also, for example, iron lines) with different excitation potential (but not saturated lines because they may have a contribution from the chrmosphere) must be fitted without changing the abundance. RHD simulations may be used to find a possible correlation with the velocity field in the atmosphere.

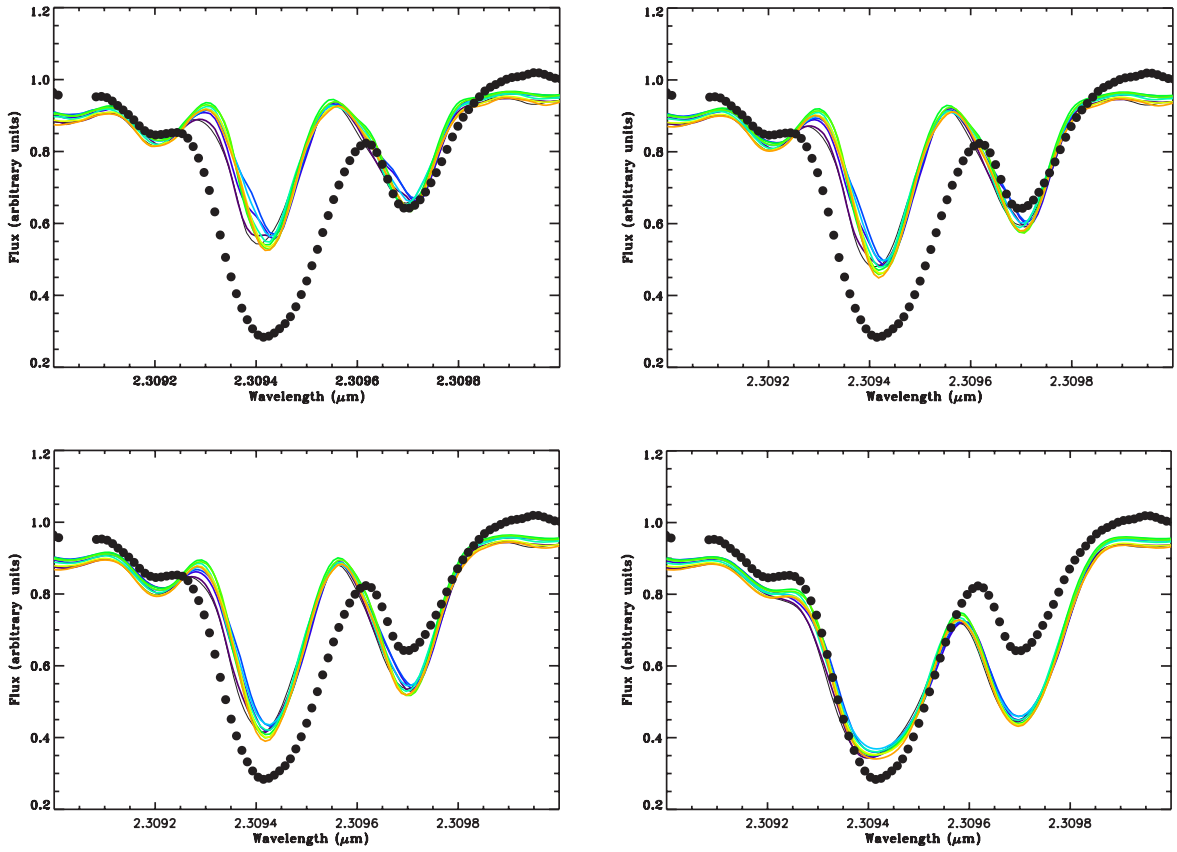

Figure 6.2: Time sequence computed for the model st35gm03n07 in Tab. 4.1 (each colors refers to a snapshots with a step of 23 days, the total time covered is about 230 days) is compared to α Ori observations by Wallace & Hinkle (1996) (dots). The microtubulence is 0 in top panel, 1.5 km/s in top right panel, 2.5 in bottom left and 5 km/s in bottom right panel. The resolution for the calculation is 1.2 km/s.

An important point of concern is the determination of the correction to the stellar center-of-mass velocity due to the convective movements in the atmosphere of RSGs. In fact, the zero point of the wavelength scale is indeterminate since the true radial velocity of the stellar center-of-mass is not known, and only relative lineshifts can be measured. One could obtain the stellar center-of-mass velocity by either (i) determining the radial velocity from astrometric observations of the parallax, the proper motions and the secular acceleration, (ii) observing stars in an undispersed galactic cluster.
RHD simulations present a unique opportunity to obtain the stellar center-of-mass velocity. For this purpose I consider the CO line with higher excitation: λ = 23057.543 Å, $\log(gf)$=-4.311 and χ=5.411 eV. Due to its high excitation, this line forms in the photosphere and can be used to study the dynamical effects of convection.
Fig. 6.3 shows two lines with different excitation potential and their bisectors: top row is the line described just above (χ=5.411 eV), while bottom row is the weaker line in Fig. 6.2 (χ=1.476 eV). Both lines are supposed to form in the photosphere. The simulations (colored curves) have been shifted by between -2.08 and 0.13 km/s for the χ=1.476 eV excitation lines and by -2.99 and -1.04 km/s for the χ=5.411 eV excitation line (Tab. 6.1) to fit the observations (dots). This displacement is due to the stellar convection. The $\Delta v = v_{1.476eV} - v_{5.411eV}$, also reported in the Table, shows that the synthetic spectra of the χ=5.411 eV excitation line are always more blue-shifted than the calculated spectra of χ=1.476 eV excitation line. While for the former spectral line the shift velocities are always negative, for the latter there are also positive shift velocities.
The average over time of the absolute shift velocity of 5.411 eV excitation line (this value corresponds to excitation potential typically of inner CCF masks) is $\sim$ 2.3 km/s and it is like the velocity of the mask C1 (see Fig. 5.9). This indicates that the mask C1 could be considered as a good indicator for the radial velocity correction.
The detailed hydrodynamics calculations carried out in RHD simulations are necessary to determine radial velocities with an accuracy much better than 1 km/s. This is of extreme interest also for the future GAIA mission.

Table 6.1: Velocity shifts of the simulation to fit the observations by Wallace & Hinkle (1996)

Snapshot (years)	1.476 eV excitation line velocity shift (km/s)	5.411 eV excitation line velocity shift (km/s)	Δv km/s
21.374	-1.82	-2.60	0.78
21.564	-1.82	-1.95	0.13
21.738	-2.08	-2.73	0.65
21.929	-2.08	-2.73	0.65
22.103	-2.08	-2.73	0.65
22.277	0.13	-2.73	2.86
22.467	-0.65	-2.73	2.08
22.657	-1.56	-2.73	1.17
22.848	0.00	-1.95	1.95
23.038	-1.56	-1.95	0.39
23.228	-0.26	-2.60	2.34
23.418	-0.26	-2.34	2.08
23.608	0.26	-1.69	1.43
23.798	-0.65	-2.48	1.83
23.988	-0.91	-2.48	1.57
24.179	-0.39	-1.04	0.65
24.369	0.26	-1.95	1.69
24.559	-1.30	-2.99	1.69
24.733	-0.78	-1.95	1.17
24.923	-0.78	-1.95	1.17

A second point concerns the bisectors. Bisectors in Fig. 6.3 show that both the higher and the lower excitation line show a marked asymmetry that spans about $\sim$2-3 km/s. The calculated (colored lines with a time-step of $\sim$65 days) are most of the time blueshifted. The calculated bisectors are redshifted only during short temporal interval for the 1.476 eV excitation line. This depends on the amount of granular/intergranular contrast. As one could expect, the high excitation line is more blueshifted than the low excitation one because it forms in the hot and blueshifted granules.
The observed bisector of the 5.411 eV excitation line is well reproduced by the simulation (top right panel), but the synthetic bisectors of the 1.476 eV excitation line has not the same trend as the observed one (bottom right panel). Thus, the velocity field of the simulation is in good agreement with the observation for layers further deep in the atmosphere where the high excitation line forms. This is also confirmed by the comparison with the TiI (Sect. 6.2.2).

A third remark is about the fact that the high excitation line (χ=5.411) exhibits a double peak during some time in the simulation. Fig. 6.4 (top frame) shows a line doubling developing during about 130 days. In the upper left panel (21.374 years) a clear doubling is visible. The component at around 0 km/s is stronger than the blushitfed one at -5 km/s. The next two frames show an equilibrium between the two components with a small predominance of the blueshited peak: a bubble of gas is rising. This is indeed visible also in the average velocity maps (red arrow in bottom frame), a blue-shifted flow appear at 21.453 years and it is noticeable for 2-3 time-steps. Then in the fourth panel

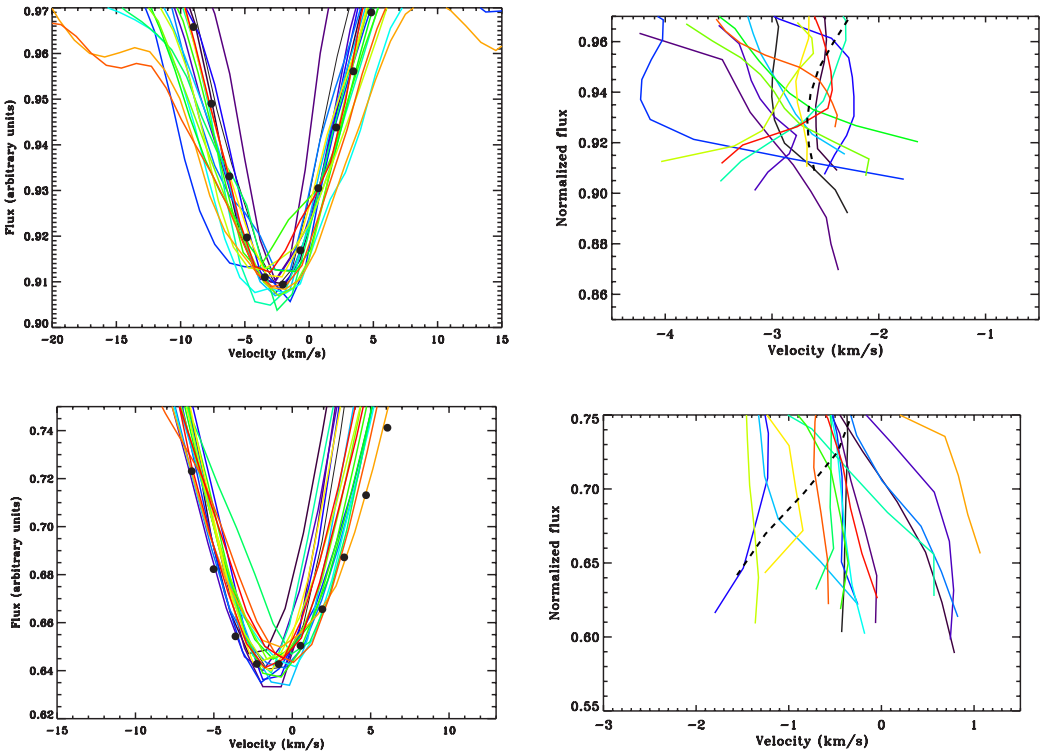

Figure 6.3: *Left column:* time sequence of calculated spectra for two high excitation first overtone CO lines (top row is χ=5.411 eV and bottom row is χ=1.476 eV). The time covered by the simulation is about 3.5 years. The resolution for the calculation is 1.2 km/s. Dots are the α Ori observation by Wallace & Hinkle (1996). *Right column:* predicted bisectors (0 km/s corresponds to rest wavelength) and dashed curve is the observed bisector.

(21.564 years) the redshifed component dominates: the upflow decelerates and cools. This double peak behavior is remarkable for about $\sim$ 130 days over the 3.5 years of simulation time, that corresponds to about 10% of the time covered.
Time monitoring of different high excitation CO lines in the infrared spectra of RSG stars would allow to check this predicted signature. The asymmetries, shifts and line doubling that are expected to be detected from observations would strongly constraint the simulations.

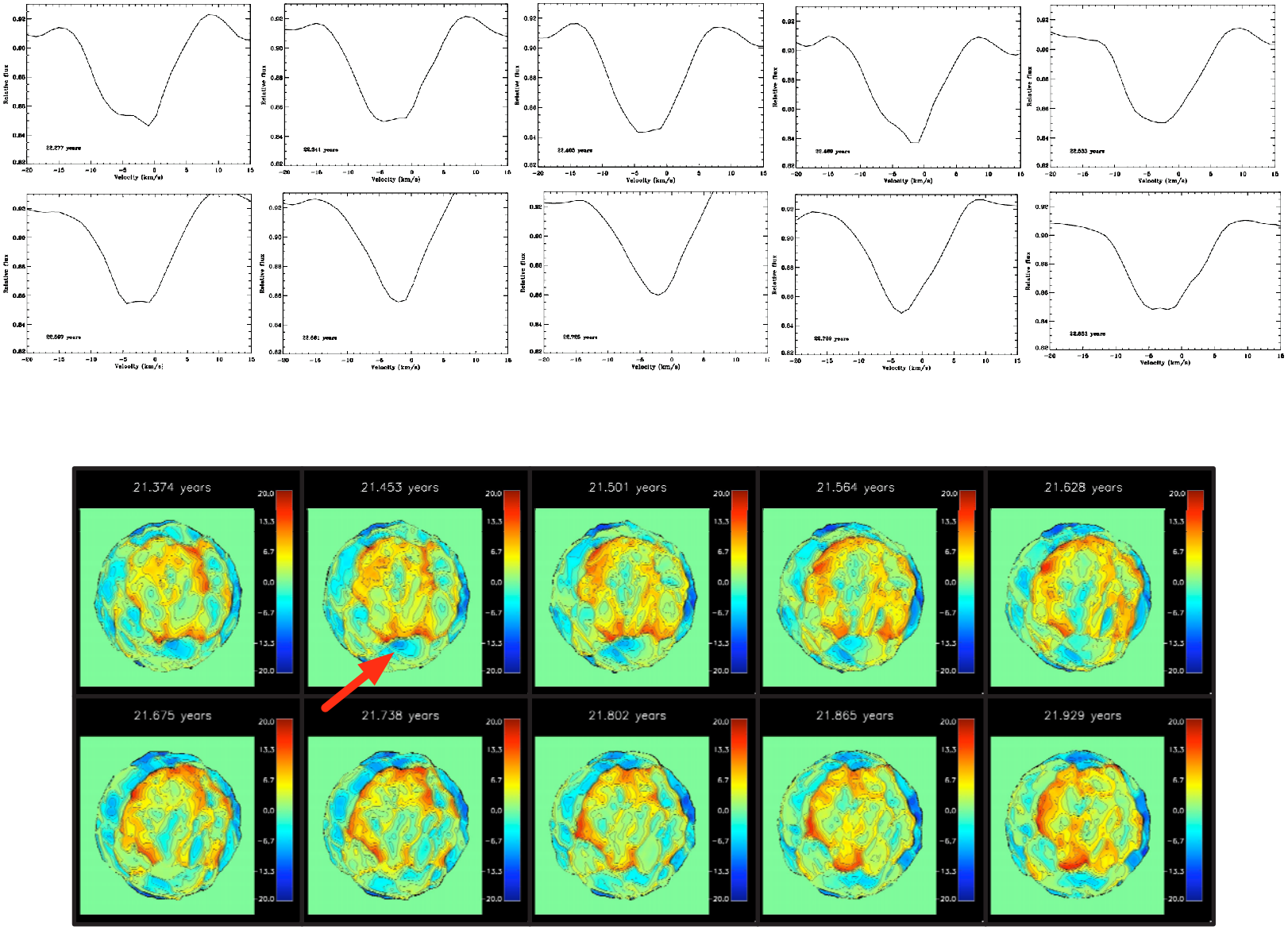

Figure 6.4: *Top box:* spectral synthesis of the double peak developing in the simulation for high excitation (χ=5.411) CO line. The time-step is about 23 days from one panel to another. *Bottom box:* velocity averaged with the contribution function (Sect. 4.1) corresponding to the same snapshots as in top box. The red arrow shows a blue-shifted flow that lasts for about 3 time-steps.

6.2.2 TiI line at 6261.11 Å

Gray (2008) presented spectroscopic observations of α Ori in the optical taken between 1996 March 23 to the end of 1999 at the Elginfield Observatory. Gray found line profiles highly variable in term of profile shape and position. He used the TiI at 6261.11 Å, with $\log(gf)$=-5.735 and χ=3.430 eV, and he probed that its half width varies from about 27 to 30.5 km/s over the course of observations. Apparently, the width is constant to that level.
Furthermore, he estimated also that the line core shifts amplitude up to 9 km/s (Fig. 6.5, top panel). Finally, he determined also the line bisector of this line, since it is sufficiently deep and possibly unblended enough (Fig. 6.5, bottom panel). From the Figure, Gray concluded that (i) shapes variations occur on the 1 km/s level, including change in curvature, reversal curvature and slope; (ii) shifts are much larger than the shape variations; and (iii) the predominant shape is like a reversed "C".

I investigated the behavior of the same spectral line in RHD simulation st35gm03n07 (Tab. 4.1). The time covered is about 550 days with a step of ∼23 days. The line profiles in Fig. 6.6 appear extremely variable with line core shifts and asymmetries like in the paper by Gray and as already pointed out by Josselin & Plez (2007). I have already mentioned this before in my thesis but I want to stress out that time variable structures are a natural consequence of giant convection cells. A direct comparison to Gray's observation line profiles would help to determine the radial velocity correction that may have to be applied to correct the observations.

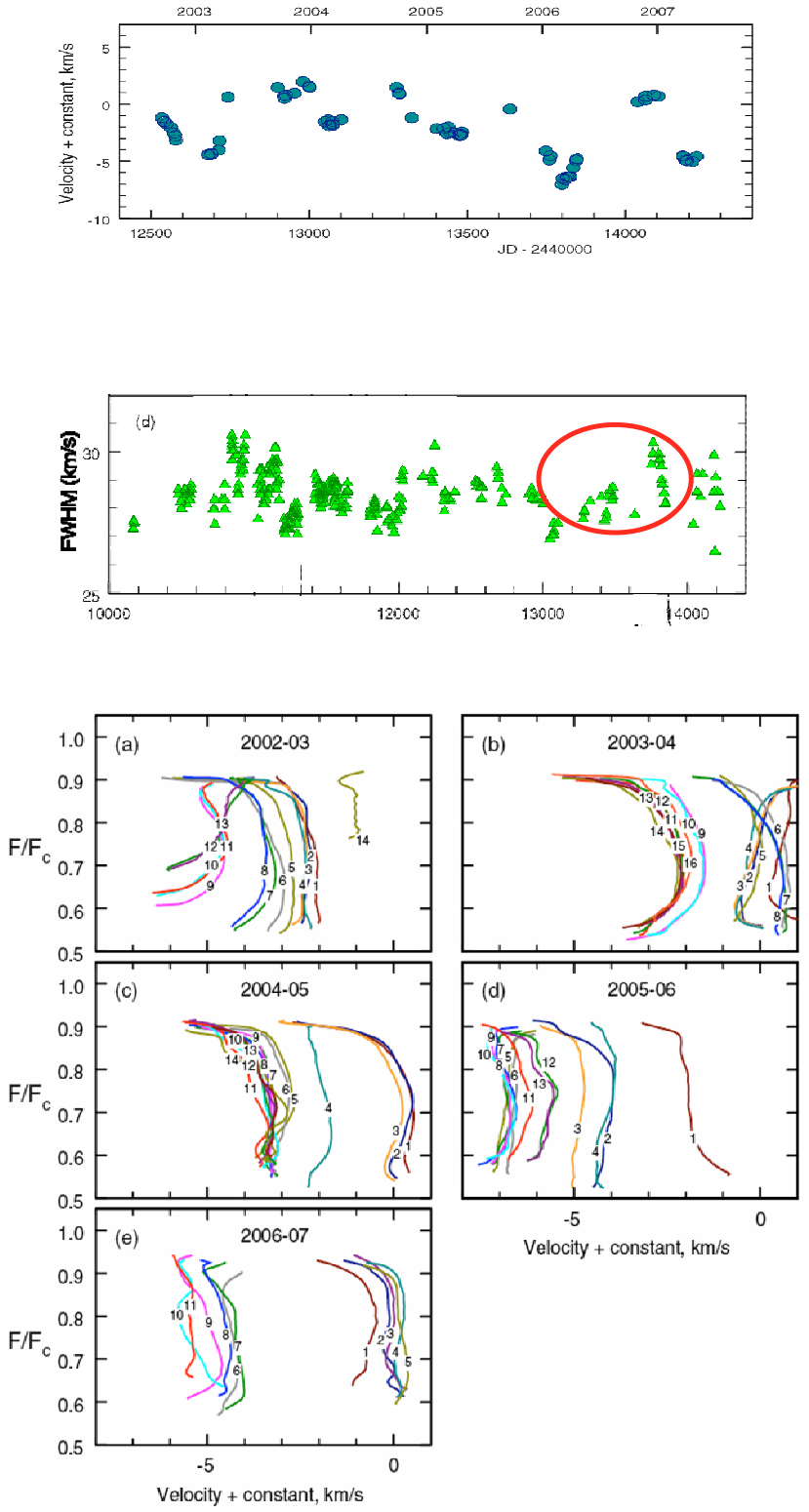

Figure 6.5: *Top penel:* Mean core velocities of three spectral lines plus an unknown constant as a function of time for α Ori observations by Gray (2008). *Central penel:* Full half width of TiI line as a function of the time. The red circles indicate a region described in the text. *Bottom penel:* Bisectors of the TiI line at 6261.11 Åfor different individual observing seasons. The position of the zero velocity is unknown. The numbers indicate the time order of the exposures. Figure from Gray (2008).

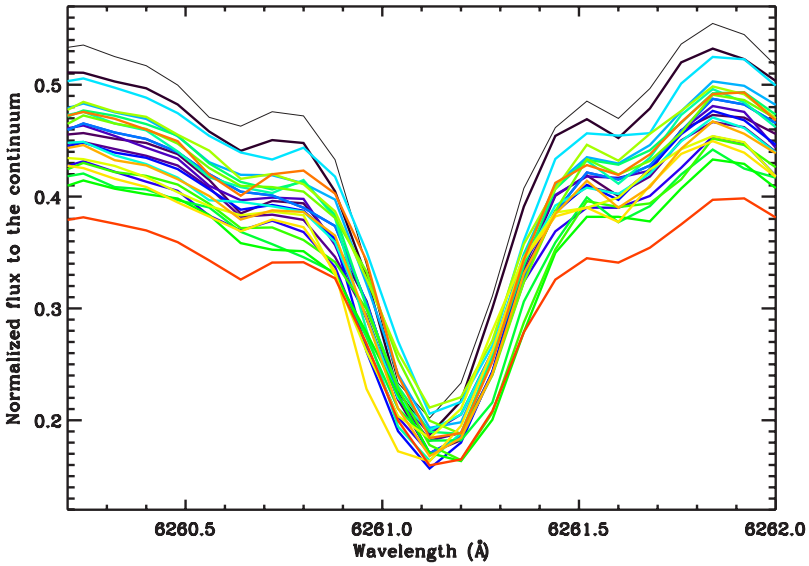

Figure 6.6: Spectral line TiI line at 6261.11 computed with RHD simulation st35gm03n07 (Tab. 4.1). The time covered is about 550 days with a step of ∼23 days from black, blue to red.

Then, I have fitted the line with a Gaussian function in order to find the core velocity position and shifts and the full width at half maximum (FWHM). Fig. 6.7 (left panel) shows the line core as a function of time and it is noticeable that the velocity range is about 3 km/s and the average velocity is 1.53±0.75 km/s at one sigma. In right panel is reported the FWHM. The large turbulent atmospheric movements broaden the spectral line up to velocities exceeding 18 km/s (18.42±3.21 km/s at one sigma) with a peak up to 30 km/s. This trend is in agreement with the observations (e.g., red circle in Fig. 6.5, central panel), but the amplitude of the measured broadening in the RHD simulation is smaller than what is observed for α Ori. This could be a consequence of the fact that the RHD simulation parameters are not exactly the same as for α Ori.

The inspection of the synthetic bisectors (Fig. 6.8) reveals that in RHD models the predominant shape is a reverse "C" shape with variations of few km/s. The line shifts are strong (up to 5 km/s, bottom panel) and larger than the shape variations. Finally, there is no consistent correlation between the shape and the shift.
This is really promising in view of the fact that for that RHD simulations do match the same trend of the observed bisectors and therefore large convective cells motions on the surface of RSG could explain them. A forthcoming paper (Chiavassa et al. 2008, in preparation) will show in detail this comparison with also the other spectral line mentioned in the paper by Gray.

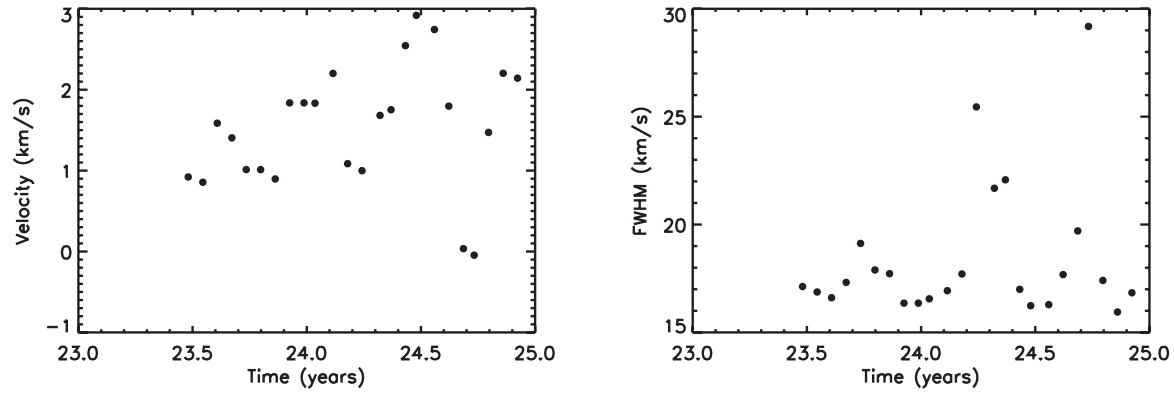

Figure 6.7: *Left penel:* TiI line (6261.11 Å) core positions as a function of the time for RHD simulation st35gm03n07 (Tab. 4.1). The total time covered is about 550 days with a step of ∼23 days. *Right penel:* line full width at half maximum as a function of the time.

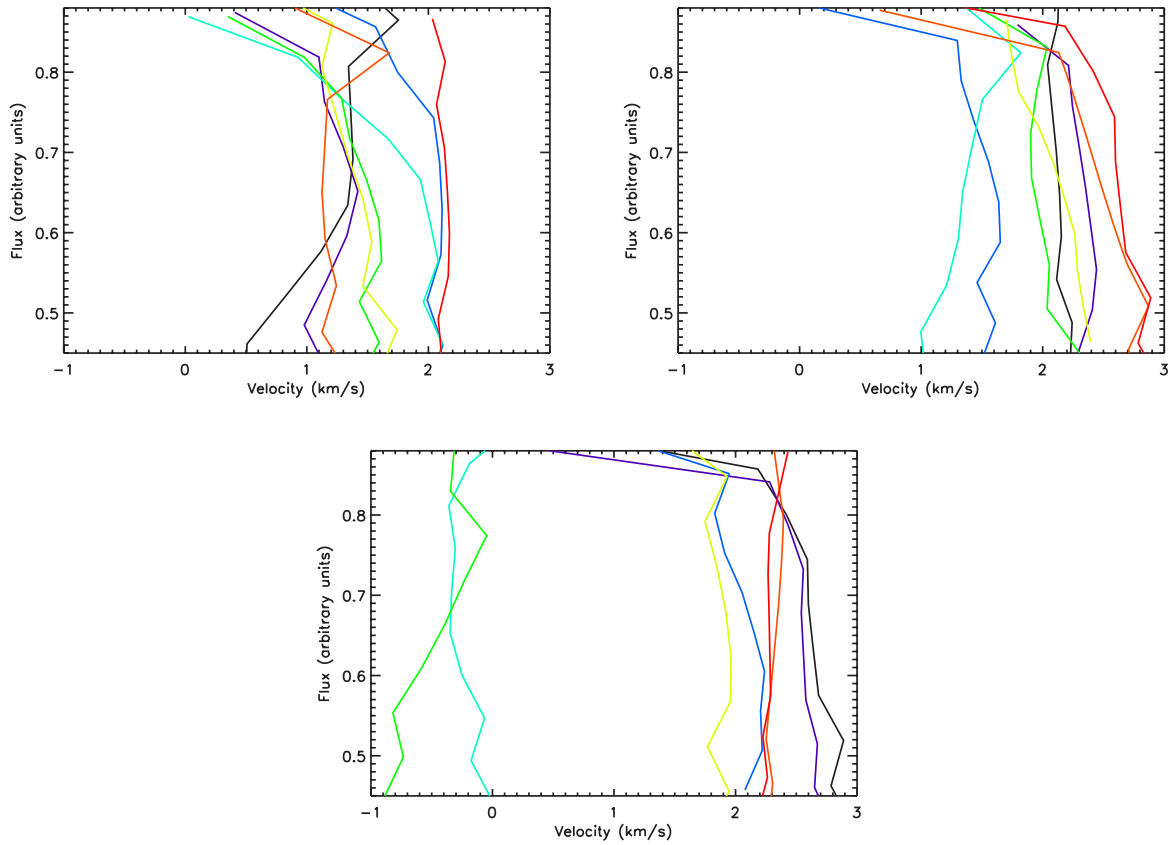

Figure 6.8: Synthetic bisectors of the line TiI line (6261.11 Å). Each panel contains 8 snapshots of the RHD simulation (about 185 days) represented by colors from black, blue to red. Top left panel covers from 23.481 to 23.925 years, top right panel from 23.988 to 24.432 years and bottom panel from 24.480 to 24.923 years.

Table 6.2: OH lines from Goldman et al. (1998)

Wavelength (cm^{-1})	Excitation potential (eV)	$\log(gf)$
814.324	1.300	-1.58
814.728	1.297	-1.56
815.403	1.302	-1.58
815.953	1.300	-1.56

6.2.3 Water vapor lines at 12.2 μ m

I present in this Section the detailed comparison of H_2O and OH lines at 12.2 μm. This region contains several water vapor lines and OH lines (Tab. 6.2). Only weak atomic lines are present. Ryde et al. (2006) underlined that this spectral region is important to constrain the MOLsphere models because the signature of water vapor lines and OH of their data are not explained by classical models or published MOLsphere models. However, Ryde et al. found that the observation is reproduced by a spectrum based on a model with a cooler (outer) photospheric temperature structure, as compared with a temperature structure calculated from a classical photospheric modeling.

I have tested if the RHD simulations are capable to reproduce these data. For this purpose, I have use the model st35gm03n07 (Tab. 4.1). I included in the opacity tables the H_2O line list of Barber et al. (2006), the OH lines as defined in Tab. 6.2 and atomic lines.

Following Ryde et al. (2006), the synthetic spectra are diluted by an extra, optically thin dust emission:

$$F_\lambda^{\rm diluted} = (1 - f_{\rm dust})\, F_\lambda + f_{\rm dust} \tag{6.1}$$

where $F_\lambda^{\rm diluted}$ is the normalized modeled flux including the dust emission, and F_λ is the normalized synthetic spectrum. The attenuation of the photospheric light through the dust is included in $f_{\rm dust}$. The dust emission contribution to the total observed flux of Ryde et al. (2006) is

$$f_{\rm dust}^{\rm thin} = (F_{\rm star+dust} - F_{\rm star}) \,/\, (F_{\rm star+dust}) = 28\% \tag{6.2}$$

for an optically thin ($\tau << 1$) circumstellar dust envelope. The observations are wavelength calibrated using telluric features in the observed spectral region (the wavelength calibration accuracy is between 0.25 to 0.5 km/s).

The spectra used for the comparison is not the same as in paper by Ryde et al., but it has been taken with the same instrument at another epoch. The spectra are from Matt Richter and they result from an average of four spectra taken on January, 18th 2001 and flattened (by B. Plez) using a spectrum of Becklin-Nengebaner object. The results is that the spectra are flattened better. This is otherwise a difficult task because the orders are very short.

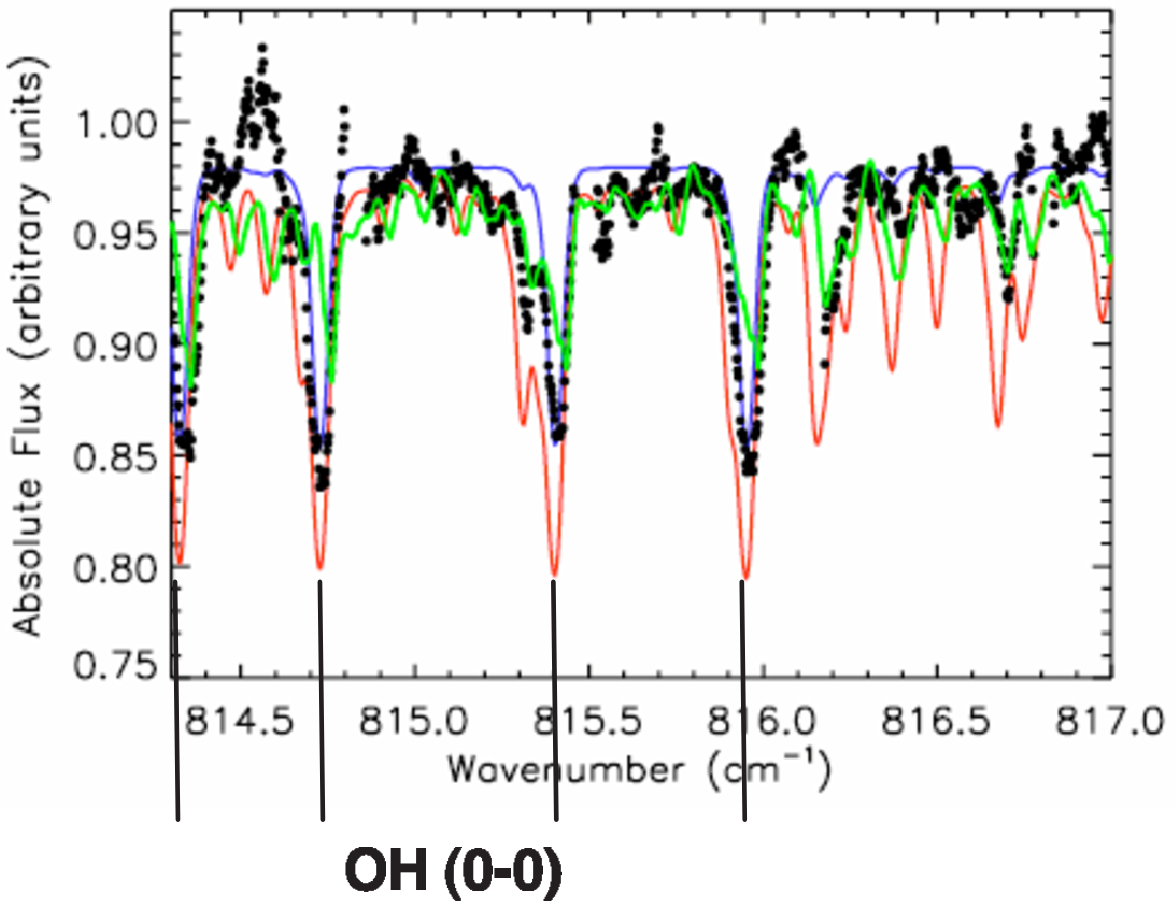

Figure 6.9: Detailed comparison at 12.2 μm with the observation (dots) by M. Richter (8th January 2001) and flattened by B. Plez using a spectrum of Becklin-Nengebaner object. The green curve is a snapshot of the RHD simulation described in the text (same snapshot used to fit TiO bands in Fig. 6.12). The blue and red curves are spectra obtained by a one-dimensional MARCS model at 3600K and 3200K, log(g)=0.0, respectively, computed with a microturbulece=3.5 km/s and convoluted with a macroturbulence of 12 km/s. The observations are in the LSR system. The OH lines reported in Tab. 6.2 are indicated. The resolution for RHD model calculation is 0.8 km/s.

Fig. 6.9 shows the comparison. The observation (black dots) shows four strong lines (OH 0-0 lines reported in Tab. 6.2) and a collection of H_2O absorption lines. The RHD simulation (green line) reproduce well the overall appearance of the water spectrum that is influenced by numerous weak water vapor lines.
However, the strong OH lines cannot be explained, even increasing the oxygen abundance of a factor 2. It should be noted that saturated lines are not as sensitive to the abundances as are weak lines.
The integrated intensity map is reported in Fig. 6.10. This map can be compared to a snapshot in Fig. 4.8 (H band) or 4.15 (K band). The surface structures appear less clear than in the near-IR but the granules and lanes are still visible.

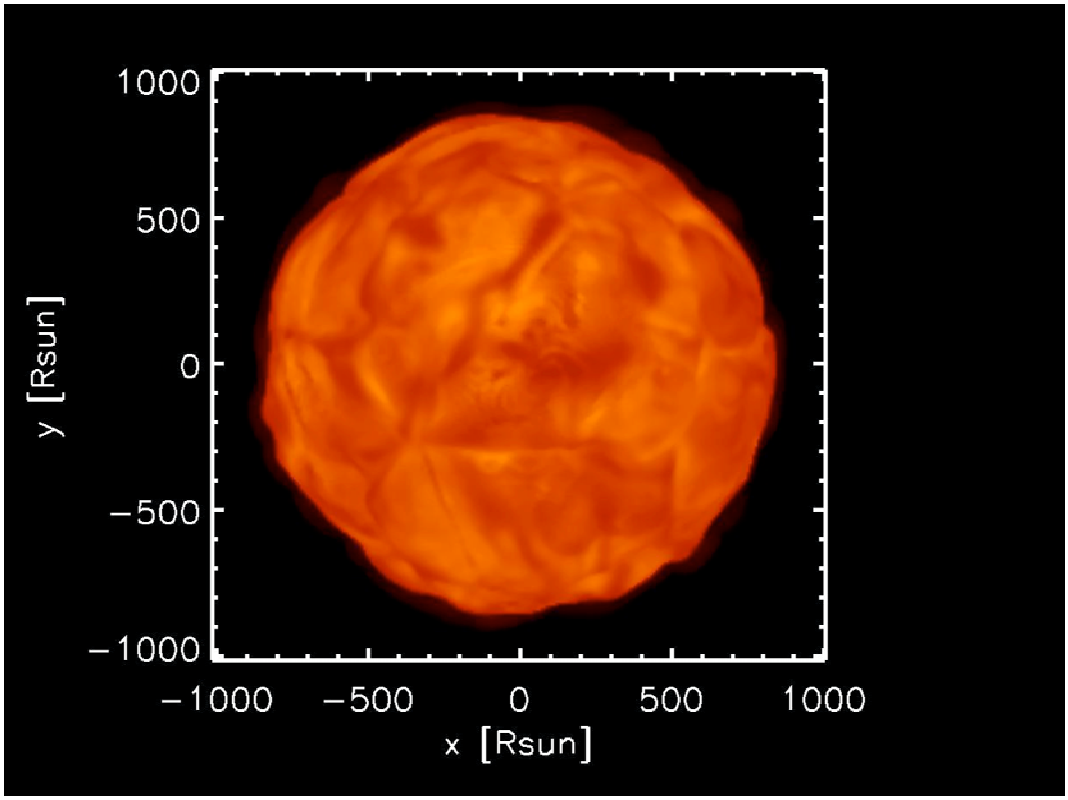

Figure 6.10: Synthetic map of the linear intensity computed in the spectral range of Fig. 6.9. The range of the intensity is [0,8] erg/s/cm^2/Å. The resolution for the calculation is 0.8 km/s.

At this point, since the RHD simulation cannot reproduce the OH lines, it is necessary to introduce the one-dimensional models that give an explanation. In Ryde et al. (2006), they used two MARCS model with different temperatures and probed that water vapor lines are more sensitive to the temperature than the OH lines. Moreover, they argued that surface inhomogeneities could explain their spectra because the cooler model could reproduce well the H_2O lines but no the OH lines, while the hotter model do the opposite. This is exactly what is shown in Fig. 6.9 with MARCS models at 3200K (red line) and 3600K (blue line).
The work is still in progress but I can try to argue some explanations for the discrepancy between the RHD model and the data. (i) In the outer layers, the temperature gradient is too shallow and this weakens the contrast between strong and weak lines. The resulting OH line saturates. The flat temperature gradient is a consequence of the grey treatment of opacities (see Sect. 4.4). (ii) The formation of some molecular opacities in scattering can lead to a selective change in equivalent widths for lines of different excitations. For TiO, Plez (1990), probed that only low excitation lines can be affected. Maybe the inclusion of

scattering could change the equivalent width of OH. (iii) The presence of a MOLsphere around the star, this test is in progress.

6.2.4 TiO bands

The electronic transition line spectrum of TiO dominates the optical spectrum of RSG stars (Fig. 1.3). In general, the blocking of radiation leads to heating up of the deeper layers of the atmosphere (backwarming).
In the upper layers of the atmosphere the situation is more complicated. For LTE, the spectral line absorption may cause a cooling of a heating depending on weather the absorption is located on the long-wavelength side of the local Planck function (cooling, e.g., H_2O in IR for late M stars) or on the short-wavelength side. In the latter case, there may be a heating if the absorption is concentrated in the upper layers (e.g., TiO in early M-star models; Krupp et al. 1978) or a cooling if the absorption is in the deeper atmosphere.
To explain this, the energy balance, when the convective flux is equal to 0, can be expressed as $\int \kappa_\lambda \left(\mathrm{J}_\lambda - \mathrm{B}_\lambda\left(\mathrm{T}\right)\right) d\lambda = \mathrm{q}_{\mathrm{rad}} - \mathrm{q}_{\mathrm{thermal}} = 0$ (e.g., Mihalas 1978), where J is the mean intensity and B the Planck function at the temperature T. Assuming LTE, the spectral lines located on the red part of the local Planck maximum tend to cool the upper layer: this is due to the fact that the intensity coming from below, J, is not greater than the local Planck function as it is little temperature dependent, in addition the intensity is reduced by the absorption of the lines themselves.Shortward of the Planck maximum the mean intensity may be greater than the local Planck function (stronger dependence on the temperature) and forces $\mathrm{q}_{\mathrm{rad}}$ and thus $\mathrm{q}_{\mathrm{thermal}}$ upwards. See Gustafsson et al. (2008) for more details.

I set up opacity tables including the TiO line list of Plez (1998) based on the best available laboratory data with the further improvements with ab-initio calculation of electronic transition moments and the inclusion of all five stable isotopes of Ti. The spectral range chosen is between 6100 and 6600 Å(TiO electronic transition is the $X^3\Delta$ to $B^3\Pi$). Fig. 6.11 shows the comparison between the calculated spectrum (black) from our best model (st35gm03n07 in Tab. 4.1) and the observed spectrum of α Ori (red). The comparison is pretty satisfactory. There is a good match of the computed and observed TiO bandstrength. However, the computed TiO bands are a little weaker than the observation and the contrast between strong and weak lines is smaller than in the observation. This is due to the too shallow temperature gradient that weakens the contrast between strong and weak lines.

In order to quantify the problem I have shown in Sect. 4.4 the difference between the temperature gradient of the MARCS one-dimensional model and the average temperature gradient of the RHD simulation. Using one-dimensional MARCS models (Plez et al. 1992 and Gustafsson et al. 2008), I have estimated to what temperature the synthetic spectrum from RHD simulation corresponds to. Fig. 6.12 shows the same synthetic spectrum (red line) used for the comparison in Fig. 6.11 over-plotted to a MARCS models (black line) at T_{eff}=3600K, log(g)=-0.5, microturbulence=2km/s, solar matellicity. The MARCS model has similar TiO bandstrengths ($\sim$ 30% stronger) to the RHD simulation and the continuum flux almost coincide (MARCS continuum is 5% higher). Thus, since the effective

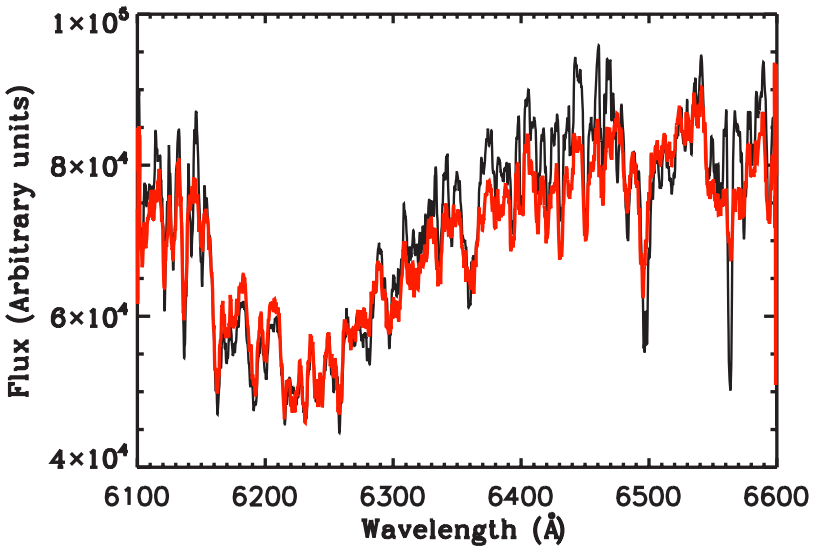

Figure 6.11: Comparison of the calculated spectrum (red) from one snapshot of the RHD simulation described in the text to the α Ori UVES (Dekker et al. 2000) observed spectra (black, Bagnulo et al. 2003). The high resolution spectra (the resolution for the calculation is 3 km/s) have been smoothed to point out the TiO bandstrengths. The TiO electronic transition is the $X^3\Delta$ to $B^3\Pi$.

temperature of the RHD simulation st35gm03n07 is $\sim$ 3495.2K, I can conclude that if I use a RHD simulation to fit the observed TiO bands (as Levesque et al. 2005) for finding the effective temperature, I would obtain an effective temperature scale cooler than what one-dimensional models show.

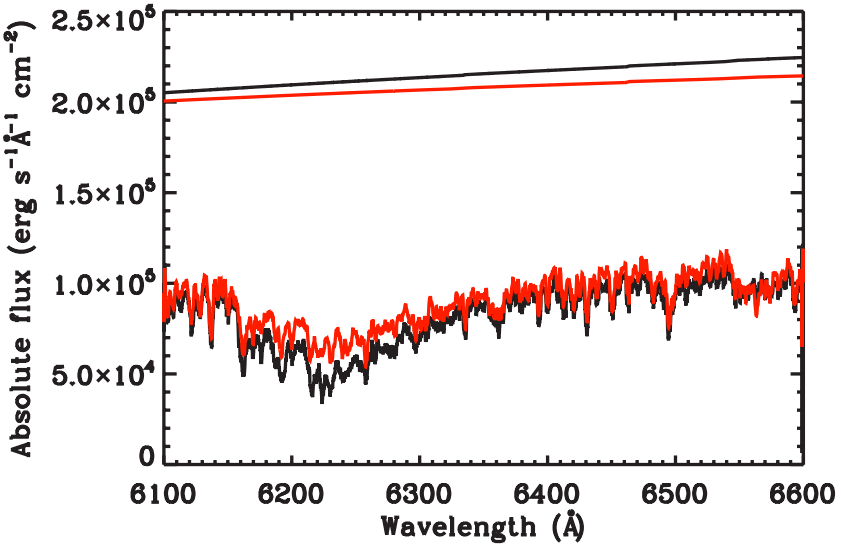

Figure 6.12: Synthetic spectrum of a MARCS model (black line, T_{eff}=3500K, log(g)=-0.5, microturbulence=2km/s, solar metallicity) used to estimate the temperature of the synthetic spectrum computed from the RHD simulation described in the text and used for the comparison with the observation (Fig. 6.11). The continuum is also plotted.